Results in Physics 22 (2021) 103933

Contents lists available at ScienceDirect

Results in Physics

journal homepage: www.elsevier.com/locate/rinp

Analysis of the magnetic field dependence of the isothermal entropy change of inverse magnetocaloric materials

L.M. Moreno-Ramírez [a], J.Y. Law [a], S.S. Pramana [b], A.K. Giri [c], V. Franco [a,*]

[a] Dpto. Física de la Materia Condensada, ICMSE-CSIC, Universidad de Sevilla, P.O. Box 1065, 41080 Sevilla, Spain
[b] School of Engineering, Newcastle University, Newcastle upon Tyne NE1 7RU, UK
[c] CCDC Army Research Laboratory, Aberdeen Proving Ground, MD 21005, USA

ARTICLE INFO

Keywords:
Inverse magnetocaloric effect
Antiferro-ferromagnetic phase transitions
Field dependence studies

ABSTRACT

In this work, the magnetic field dependence of the inverse magnetocaloric (MC) effect is analyzed using a mean field approach for describing antiferromagnetic to ferromagnetic magnetoelastic transitions. The model is able to describe both second- and first-order transition through the introduction of a magnetovolume energy term. The power law dependence for the field dependence of the isothermal magnetic entropy change ($\Delta S_{iso} \propto \Delta H^n$), has an exponent n with an overshoot above 2 for first-order transitions, while it is not present for the second-order case. This is in excellent agreement with previous phenomenological observations, supporting the validity of recently proposed criterion to distinguish between first- and second-order thermomagnetic transitions. A main difference with respect to direct MC effect is that negative values of the exponent n are obtained at temperatures close to the transition. This is ascribed to the reduction of the inverse MC response due to the influence of the unavoidable ferromagnetic to paramagnetic transition at higher temperatures. The obtained features are qualitatively compared to those of $GdBaCo_2O_6$ (antiferromagnetic to ferromagnetic magnetoelastic transition), showing a good agreement between both experiments and the model. The obtained information is extrapolated to understand the behavior of the exponent n for a $Ni_{49}Mn_{36}In_{15}$ sample (magnetostructural transition).

Introduction

Solid-state magnetic refrigerators attract the attention of the research community since G. V. Brown explored this technology as a real alternative to the conventional systems at room temperature [1], being more energy efficient and less-contaminant than its gas compression-expansion based counterpart [2,3]. This technology is based on the magnetocaloric (MC) effect, which is defined as the temperature (or magnetic entropy) change produced by the application or removal of a magnetic field in adiabatic (or isothermal) conditions, ΔT_{ad} (or ΔS_{iso}) [4]. However, this technology is not only limited to room temperature applications being cryogenic applications still on demand (e.g. molecular coolers [5] or rare earth based alloys and oxides [6–10]). Since the device of G. V. Brown, the interest on room temperature MC materials has evolved [11]: from Gd [12], which undergoes a second-order transition, to different families of materials as GdSiGe [13], LaFeSi [14], MnFeP [15], Heusler [16] undergoing first-order transitions. Classifying MC materials according to the order its thermomagnetic transition [17], first-order materials show larger MC values than typical second-order materials, however the response of these materials is reduced under cycling conditions due to the irreversibility of the response (while for second-order ones the response is fully reversible) [18]. Therefore, the appropriate knowledge of the order of the transition has not only importance from the fundamental point of view, but it is also needed in order to know to which extent the response of the materials can be optimized for device applications.

The studies based on the analysis of the field dependence of the MC effect allow to obtain relevant and useful information from thermomagnetic transitions. First, these studies were applied in materials undergoing second-order ferromagnetic (FM) to paramagnetic (PM) transitions [19]. In this type of transitions, the studies allow to extract information of the critical behavior in the region close to the transition (e.g. critical exponents of the transition [20], a master curve for ΔS_{iso} [21], the Curie temperature [22] and many others). In recent works, the field dependence of the MC effect in materials undergoing first-order transitions has been explored, leading to a quantitative criterion that allows identifying first-order transitions through the existence of an overshoot of $n > 2$ in the field dependence exponent ($\Delta S_{iso} \propto \Delta H^n$), while

* Corresponding author.
E-mail address: vfranco@us.es (V. Franco).

https://doi.org/10.1016/j.rinp.2021.103933
Received 20 December 2020; Received in revised form 14 January 2021; Accepted 31 January 2021
Available online 4 February 2021

the overshoot is not observed for second-order ones [23]. This phenomenological criterion has been successfully applied to different families of MC materials of both direct and inverse type (i.e. those with $\Delta S_{iso} < 0$ or $\Delta S_{iso} > 0$ upon magnetization, respectively). For direct MC effect, the overshoot feature for fingerprinting first-order transitions can be validated in the frame of the Bean-Rodbell model [24], obtaining an excellent agreement between experiments (materials that undergo a FM to PM magnetoelastic transition such as LaFeSi) and the model [23,25,26]. However, for inverse MC effect the validity of the proposed criterion and the characteristics of the field dependence have only been studied experimentally [23,27,28]. In order to extend the applicability of this phenomenological criterion beyond experimentation, its validity has to be further supported by a model that describes the features of inverse MC materials. This inverse effect is caused by an increment of the magnetization with temperature and it is typical of antiferromagnetic (AF) to FM transitions (e.g. in AF superconductors [29,30], FeRh [31,32] or Mn_3GaC [33] alloys) or magnetostructural transitions (e.g. in Heusler alloys [34]).

In this work, we extend the field dependences studies to the case of magnetoelastic AF to FM transitions using a mean-field approach (Landau type). Although these approximations have been previously employed to qualitative illustrate the magnetic behavior of different systems (Heusler or FeRh alloys), the first-order character due to magnetovolume effects was not reported [35,36] and also the field dependence character of the isothermal magnetic entropy change was not considered. To extend the models used in the literature, a magnetovolume term is phenomenologically proposed to obtain a volume expression according to the Callen-Callen theory [37]. Using this model, we are able to reproduce the experimentally observed features for the exponent n, showing the existence of the characteristic overshoot for first-order transitions and its absence for second-order ones. This supports the extension of the quantitative criterion to AF-FM phase transitions and set the basis for the analysis of the exponent n in these materials. It is shown that the model shows negative values for the exponent n at temperatures close to the transition temperatures, due to the influence of the FM to PM transition produced at higher temperatures (which is unavoidable) which leads to a decrease of the ΔS_{iso} values associated to the AF to FM transition. These features (overshoot and negative values close to the transition) have been compared to those of experimental measurements for $GdBaCo_2O_6$ [38] undergoing a magnetoelastic first-order AF to FM transition, finding a good agreement between experiments and modeling. Moreover, the analysis can also be used to understand the field dependence characteristics for $Ni_{49}Mn_{36}In_{15}$ [39] alloy that shows an inverse MC effect associated to a martensitic transition.

Model of a magnetoelastic AF to FM transition

For modeling a magnetic material, the Gibbs free energy (G) is expressed as the sum of the different energy terms associated to the different subsystems of the material, mainly magnetic and lattice ones [40]:

$$G = G_M + G_V + G_{MV}, \tag{1}$$

where G_M is the magnetic contribution, G_V the volume contribution and G_{MV} takes into account the cross effect between both subsystems (i.e. the magnetovolume term).

First, we are going to focus on the magnetic contribution. For an AF material, in the mean field approach, the total magnetization ($\boldsymbol{M}$) of the system is expressed as the sum of two equal magnetic subsystems with opposite directions (denoted as 1 and 2). With this, G_M is formulated as [41]:

$$G_M = \frac{W'}{2}\left(\boldsymbol{M}_1^2 + \boldsymbol{M}_2^2\right) + W\boldsymbol{M}_1\boldsymbol{M}_2 - (\boldsymbol{M}_1 + \boldsymbol{M}_2)\boldsymbol{H} - TNk_B\left(\int_0^{|\boldsymbol{M}_1|/M_S} \mathrm{B}^{-1}(x)dx + \int_0^{|\boldsymbol{M}_2|/M_S} \mathrm{B}^{-1}(x)dx\right), \tag{2}$$

where $\boldsymbol{M}_1$ and $\boldsymbol{M}_2$ are the magnetization vector of the magnetic sublattices 1 and 2, M_s the saturation magnetization of each of the sublattices, W' the exchange constant between the moments of the same sublattice, W the exchange constant between the moments of the different sublattices, $\boldsymbol{H}$ the magnetic field, T the temperature, N the number of magnetic moments in each of the sublattices, k_B the Boltzmann constant and B^{-1} the inverse Brillouin function. **Eq. (2)** can be simplified considering that both sublattices have the same magnetization modulus ($|\boldsymbol{M}_1| = |\boldsymbol{M}_2| = M'$) and that the magnetic field is applied perpendicular to both sublattices (following the symmetry of the G_M term [41]). Then, the magnetization vectors of the different subsystems can be expressed as a function of the angle between the magnetization and field directions ($\pi/2$-θ), being:

$$\boldsymbol{M}_1 = M'\cos\theta\ \vec{i} + M'\sin\theta\ \vec{j}, \tag{3}$$

$$\boldsymbol{M}_2 = -M'\cos\theta\ \vec{i} + M'\sin\theta\ \vec{j}. \tag{4}$$

According to this, the total magnetization is $\boldsymbol{M} = 2M'\sin\theta\ \vec{j}$. Introducing **Eqs. (3)** and **(4)** in **Eq. (2)**, then G_M is expressed as [41]:

$$G_M = W'M'^2 - WM'^2\cos 2\theta - 2M'\sin\theta H - 2TNk_B\int_0^{M'/M_S} \mathrm{B}^{-1}(x)dx, \tag{5}$$

which is a function of both M' and θ.

Second, for the volume contribution to the Gibbs free energy, we assume an elastic approach as for other models like Bean-Rodbell [24]:

$$G_V = \frac{\omega^2}{2K} + p\omega, \tag{6}$$

where ω is the relative volume change, K is the compressibility of the material and p the pressure. In this study we are not going to consider pressure effects and then $p = 0$ (the consideration of this pressure just would lead to the addition of p in **Eq. (10)**, being just a shift in the case of constant pressure that would not affect the results).

Third, for the magnetovolume term, it can be proposed that is proportional to relative volume change times the total magnetization to the square power:

$$G_{MV} = -\frac{\beta}{4}\omega M^2 = -\beta\omega M'^2(\sin\theta)^2, \tag{7}$$

being β the magnetovolume coupling constant.

Finally, according to the previous magnetic (**Eq. (5)**), volume (**Eq. (6)**) and magnetovolume terms (**Eq. (7)**), the Gibbs free energy becomes:

$$G = W'M'^2 - WM'^2\cos 2\theta - 2M'\sin\theta H - 2TNk_B\int_0^{\frac{M'}{M_S}} \mathrm{B}^{-1}(x)dx + \frac{\omega^2}{2K} - \beta\omega M'^2(\sin\theta)^2, \tag{8}$$

being function of M', θ and ω. These magnitudes can be obtained through the minimization of G. Minimizing G with respect to ω :

$$\frac{\partial G}{\partial \omega} = \frac{\omega}{K} - \beta M'^2(\sin\theta)^2 = 0, \tag{9}$$

leads to:

$$\omega = K\beta M'^2(\sin\theta)^2 = K\beta M^2 \tag{10}$$

This dependence is similar to the one of the Callen-Callen theory [37]

though extended to the AF state. To obtain the other 2 magnitudes, **Eq. (10)** is introduced in **Eq. (8)**, being the latter one dependent on $M^{'}$ and θ:

$$G = W^{'}M^{'2} - WM^{'2}\cos 2\theta - 2M^{'}\sin\theta H - 2TNk_B\int_0^{\frac{M^{'}}{M_S}} \mathrm{B}^{-1}(x)dx - \frac{1}{2}K\beta^2 M^{'4}(\sin\theta)^4. \tag{11}$$

To obtain the equilibrium condition of our model system, we have to minimize with respect θ and $M^{'}$ variables, however the solution becomes quite complicated. As an approximation, we can assume that the $M^{'}$ value is the one obtained from the Brillouin solution. Then, we just have to find the solution for θ, minimizing G with respect θ we get:

$$\frac{\partial G}{\partial \theta} = 4WM^{'2}\cos\theta\sin\theta - 2M^{'}H\cos\theta - 2K\beta^2 M^{'4}(\sin\theta)^3\cos\theta = 0, \tag{12}$$

which after rearrangement, is expressed as:

$$2M^{'}\cos\theta(2WM^{'}\sin\theta - H - K\beta^2 M^{'3}(\sin\theta)^3) = 0. \tag{13}$$

It is worth noting that, up to the moment, the material is in the AF state in the whole temperature range and the AF to FM transition is just caused by the application of a magnetic field. To introduce the AF to FM transition even in the absence of magnetic fields, a phenomenological equation for the exchange constant between the different subsystems is assumed:

$$W = W_0\left(\frac{T_0 - T}{T_0}\right), \tag{14}$$

being W_0 a constant and T_0 the AF to FM transition temperature at 0 field. This **Eq. (14)** is introduced in **Eq. (13)**, having an equation to describe AF to FM magnetoelastic transitions.

$$2M^{'}\cos\theta\left(2W_0\left(\frac{T_0 - T}{T_0}\right)M^{'}\sin\theta - H - K\beta^2 M^{'3}(\sin\theta)^3\right) = 0. \tag{15}$$

From **Eq. (15)**, the magnetization of the material can be obtained in both FM and AF states. It can be observed that $\theta = \pi/2$ corresponds to the FM state, which leads to the total magnetization $\boldsymbol{M} = 2M^{'}\vec{j}$ for fields above the critical field (H_C):

$$H_C = 2WM^{'} - K\beta^2 M^{'3}. \tag{16}$$

In the case of the AF state, which is obtained for fields below H_C, the solution for θ ($0 \le \theta < \pi/2$) is numerically obtained from:

$$2WM^{'}\sin\theta - K\beta^2 M^{'3}(\sin\theta)^3 = H. \tag{17}$$

In this way we obtain the temperature and field dependence of magnetization and ΔS_{iso} produced by the application of a magnetic field is calculated as:

$$\Delta S_{iso}(0\rightarrow H) = \mu_0\int_0^H \left(\frac{\partial M}{\partial T}\right)_{H^{'}} \mathrm{d}H^{'}. \tag{18}$$

Alternatively, ΔS_{iso} could also be derived from G, but the use of **Eq. (18)** is more appropriate for our purposes. For studying the field dependence of ΔS_{iso}, a power law dependence ($\Delta S_{iso} \propto \Delta H^n$) is typically assumed, where the exponent n is calculated according to:

$$n(T, \Delta H) = \frac{\mathrm{d}ln(|\Delta S_{iso}|)}{\mathrm{d}ln(\Delta H)}. \tag{19}$$

Experimental

In order to check the features of the model on real materials, the field dependence of the MC effect of two types of samples were studied: a $GdBaCo_2O_6$ cobaltite oxide (GBCO) undergoing a first-order magnetoelastic AF to FM transition and a $Ni_{49}Mn_{36}In_{15}$ (NiMnIn) Heusler alloy that undergoes a magnetostructural transition from a low magnetization FM state to other FM state with higher magnetization (which also present an inverse MC effect). ΔS_{iso} and exponent n have been calculated according to **Eqs. (18)** and **(19)** from magnetization measurements using discontinuous protocols [42] performed in a Lakeshore 7407 vibrating sample magnetometer with a maximum applied field of 1.5 T (cobaltite sample) and in a Quantum Design Physical Property Measurement System (PPMS) with a vibrating sample magnetometer option with a maximum applied field of 90 T (Heusler sample). Further details of the sample synthesis and characterization can be found in [28] and [27].

Results and discussion

Numerical calculations

Our objective is to understand the main features associated to the AF to FM transition, without the fitting to a determined material. For the numerical analysis we used the following parameters: J = 1.5, g = 2, M_S = 0.5·10^6 A/m; density = 10000 kg/m^3, T_0 = 300 K; K = 10^{-14} N/m^2. These parameters have been chosen in order to reproduce a material with significant MC properties at room temperature with conventional bulk magnetization values. In addition, $W_0 = 150$ and T_C = 600 K are also selected although these parameters will be further modified in order to explore its role on the properties.

First, we will show the type of transition that we can reproduce with the used model. Taking into account that the total magnetization is $M = 2M^{'}\sin\theta$, **Eq. (17)** can be written as:

$$\frac{H}{M} = W - \frac{K\beta^2}{8}M^2. \tag{19}$$

Applying the Banerjee's criterion, for which negative slopes in the H/M vs M^2 representation implies a first-order transition (while the opposite indicated second-order type), we can infer that as long as the β parameters differs from zero, the order of the transition becomes of first-order.

The effect of the magnetovolume β parameter on both magnetization and the relative volume change can be observed in Fig. 1(a) and (b),

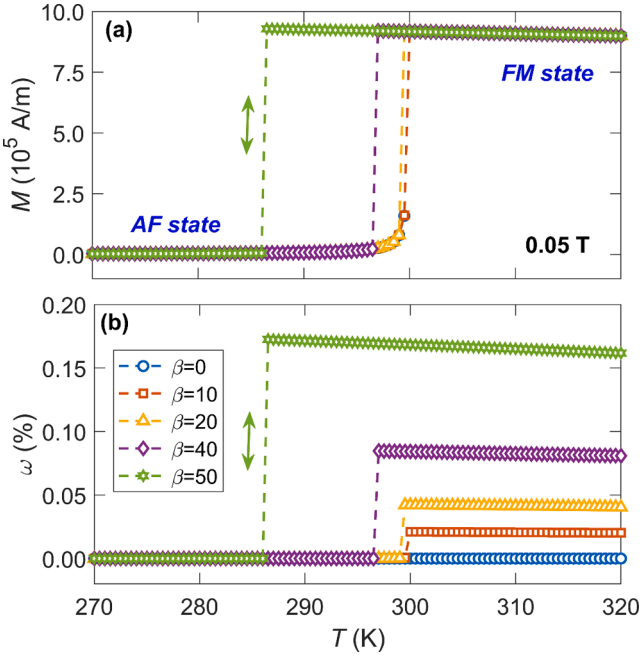

Fig. 1. Temperature dependence of the magnetization (a) and relative volume change (b) close to the transition temperature for different values of the magnetovolume coupling parameter β.

respectively, which shows the temperature dependence of both magnitudes for low magnetic field. It can be observed how the behavior of the transition is well described within the model used, with an increase in magnetization and relative volume as temperature increases above a certain transition temperature (T_t). This transition temperature is shifted to lower temperatures as β parameter increases. This is the opposite behavior already observed for the Bean-Rodbell model, for which the magnetovolume coupling parameter trends to shift the transition to higher temperatures. The transition temperature is the same for both magnetization and relative volume change. Moreover, it can be observed that the discontinuous change occurring at the transition increases with increasing β, being more significant for ω than for M. Experimentally, for magnetoelastic transitions the volume change around 1–2%, range that can be easily covered with the model presented here.

For the following description we have chosen $\beta = 40$ as an example to illustrate the behavior of the first-order transition described with the model (other selection, as 20 or 80, would not alter the conclusions). The temperature dependence of both magnetization and relative volume change in the temperature range of the transition range are illustrated in Fig. 2**(a)** and **(b)**, respectively. It can be observed how the transition temperature is linearly shifted to lower temperatures as the magnetic field increases (at a rate of 1.75 K/T for the parameters used). This rate can be tuned by the modification of W_0. This behavior is in agreement with experimental results, in which the phase with higher magnetization (which correspond with higher volume one in the model) is stabilized with increasing magnetic field. The origin of this behavior is ascribed to the assumption made in **Eq. (15)**, which implies a close to linear behavior for the critical field with the temperature, as shown in Fig. 2 **(c)**. The effect of the β parameter does not significantly modify the linear field dependence of the transition temperatures but just shift the transition temperatures to lower temperatures (see **Eq. (14)**). This relation can be tuned by assuming a different phenomenological W, however our approximation qualitatively reproduces the observed experimental behavior.

Using the modeled magnetization data, ΔS_{iso} is calculated according to **Eq. (18)**. Fig. 3**(a)** shows the temperature dependence of ΔS_{iso} at a magnetic field change of 2 T for different values of β. It can be observed that the AF to FM transition leads to an inverse MC effect (positive values of the ΔS_{iso} when applying a magnetic field) for which the maximum value increases with increasing β. After the maximum of ΔS_{iso} is reached, the values abruptly decrease to negative values associated to a direct MC effect due to the FM to PM transition. For temperatures lower than the peak, a decrease down to 0 is observed, which became more abrupt as β increases. The width of the transition is slightly reduced with increasing β; however, larger values of the refrigerant capacity can be obtained as β increases due to the larger value of the peak. It should be noted that the ΔS_{iso} values are slightly higher than experimentally reported (as also happens in the Bean-Rodbell model); this can be ascribed to the artificially abrupt change produced at the transition within this model. This high value can be lowered, resembling experimental results, by considering a transition temperature distribution and a kinetic process for the AF to FM transition, as these two characteristics are inherent to real materials.

In order to focus on the field dependence characteristics of the MC responses associated to the AF to FM transition, we calculated the exponent n according to **Eq. (19)**. It is worth noting that this magnitude is, in general, a function of temperature and magnetic field. Fig. 3**(b)** shows the temperature dependence of the exponent n at a magnetic field change of 2 T for different values of β. To describe the different features, we can distinguish different temperature ranges. At temperatures above the transition, the material is in the FM state for any applied magnetic field change and, therefore, the exponent n corresponds to that of pure

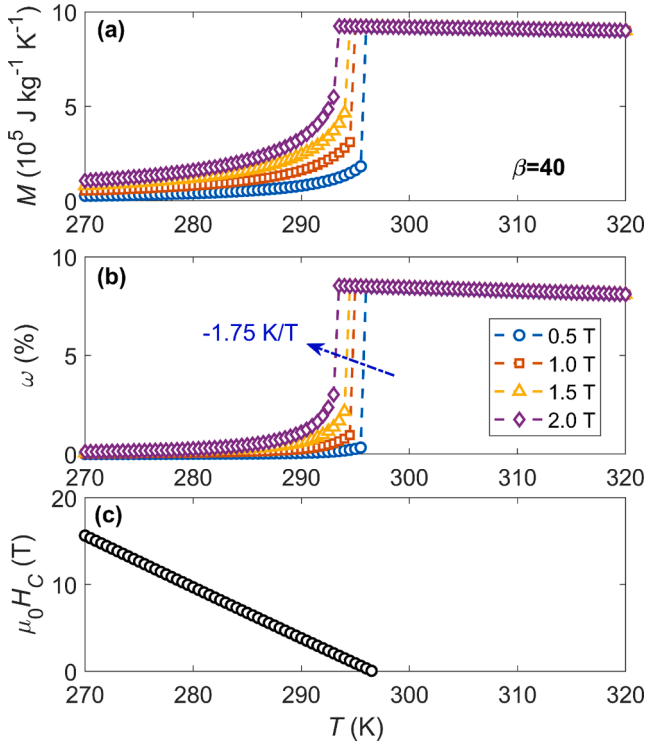

Fig. 2. Temperature dependence of the magnetization (a), relative volume change (b) and critical magnetic field (c) using $\beta = 40$ for different magnetic field.

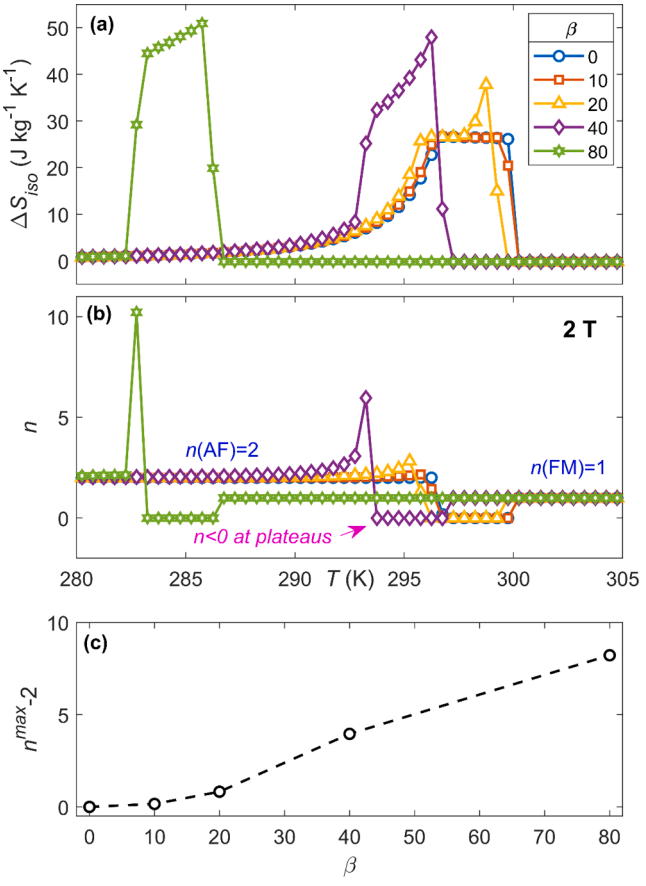

Fig. 3. Temperature dependence of ΔS_{iso} (a) and n (b) for different values of the magnetovolume coupling parameter β. (c) Maximum value of the overshoot of exponent n above 2 as a function of the magnetovolume coupling parameter β.

FM materials ($n = 1$). At temperatures close but below the transition at 0 T, a plateau of negative values rather close to 0 (≈ -0.05) can be observed. At lower temperatures, the values of n rapidly increase up to values larger than 2 in the case of $\beta = 0$, while for $\beta = 0$ n does not reach values above 2. This agrees with the quantitative criterion recently proposed [23], indicating the existence of the overshoot for first-order transitions, while it is not present for second-order ones. This feature is illustrated in Fig. 3**(c)** for which the maximum values of $n-2$ are represented as a function of β. It can be clearly observed how the maximum values increase as β increases being$n = 2$ just for $\beta = 0$. For temperatures lower than the overshoot, n values tend to the limit of 2, which corresponds to the pure AF state.

To understand the values of exponent n in the region close to the transition, we illustrate in Fig. 4 the temperature dependence of ΔS_{iso} and n for different magnetic field changes keeping $\beta = 40$. For ΔS_{iso}, it can be observed that the magnetic field trends to extend the magnetocaloric peak to lower temperatures. This is ascribed to the evolution of the transition temperature with the magnetic field. However, this is not the only cause for the overshoot as it was mentioned that the existence of such shift is not affected by β (for second-order transitions there also exists a shift of the transition temperature). Together with this, a large evolution of the ΔS_{iso} values at certain temperature with small variation of the magnetic field change should exist. This happens at the low temperature tail of ΔS_{iso} and is in agreement with the position of the overshoot in Fig. 4(b), which follows the position of the low temperature tail of the ΔS_{iso} curves, being shifted to lower temperatures as the magnetic field increases. The maximum values of n follow a non-monotonic trend with the magnetic field: increase at low magnetic fields up to a maximum value obtained at moderate fields, followed by a decrease from that maximum values. Ideally, for high enough magnetic fields the first-order characteristics are attenuated, behaving the material as a second-order one and then the overshoot would not be observed. It should be mentioned that the scattered evolution of the maximum values with magnetic field is ascribed to the discretization of the temperature axis (which is chosen similar to those of fine experimental measurements) and the narrow width of the overshoot curve. With respect to the plateau of n with negative values close to 0, it can be ascribed to the saturation of ΔS_{iso} after the first-order transition is produced. The temperature range of the plateau is the same for which the ΔS_{iso} response remains almost invariant with magnetic field. The negative values are ascribed to the direct MC effect of the FM to PM transition which is produced after the AF to FM transition and reduces the inverse response associated to the mentioned transition (opposite ΔS_{iso} signs).

The behavior of the exponent n can be also studied as a function of the magnetic field change. Fig. 5(a) and (b) illustrate the magnetic field dependence of the ΔS_{iso} and n, respectively, using $\beta = 40$ for different temperatures below the transition temperature at 0 field. For ΔS_{iso}, it can be observed that the magnetic field produces an evolution from small values that correspond to the AF state towards high values which are ascribed to the AF to FM transition. The magnetic field at which the abrupt increase of ΔS_{iso} takes place is dependent on temperature, being the critical field larger as the temperature is lower (in agreement with the critical behavior shown in Fig. 2(c)). After that, the values slightly decrease when the material is in the FM state due to the direct MC effect associated to this phase. With respect to exponent n and its behavior in these different regions, when the material is in the pure AF state and ΔS_{iso} values are small, n is equal to 2 (increasing slightly as the temperature gets closer to the transition). After that, there is an abrupt increase of n, which corresponds with the abrupt increment of ΔS_{iso}. During the whole magnetic field range in which ΔS_{iso} rapidly increases, the value of n remains above 2, being the previously mentioned overshoot produced by first-order transitions. When the material is in the FM state, the n decreases down to negative values ($\cong -0.05$) due to the small decrease of the ΔS_{iso} values in that temperature range. Finally, it can be noted that the overshoot values decrease as the transition temperature becomes smaller, as previously observed in the temperature dependence analysis.

In addition to the β parameter, another important parameter for the model is W_0. This parameter is related to the temperature dependence of the AF to FM transition and strongly affects the critical field, H_C, values (see **Eq. (14)**). Fig. 6**(a)** and **(b)** shows the temperature dependence of ΔS_{iso} and n for 2 T, respectively, and Fig. 6**(c)** shows H_C for different values of W_0 (75, 150, 300 and 450) keeping $\beta = 40$. The maximum values of ΔS_{iso} increase as W_0 increases, but this is accompanied by a reduction of the width of the peak (changing the shape from squarish to caret-like). With respect to n, the maximum values of the overshoot

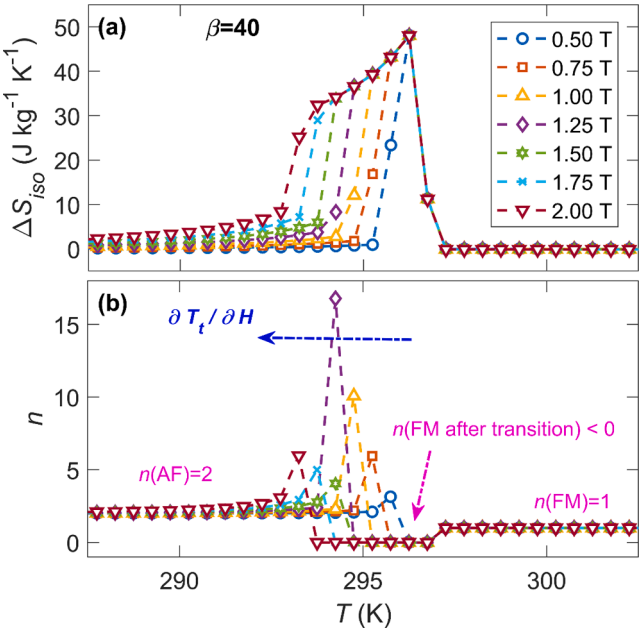

Fig. 4. Temperature dependence of the isothermal magnetic entropy change (a) and the exponent n (b) using $\beta = 40$ for different magnetic field changes.

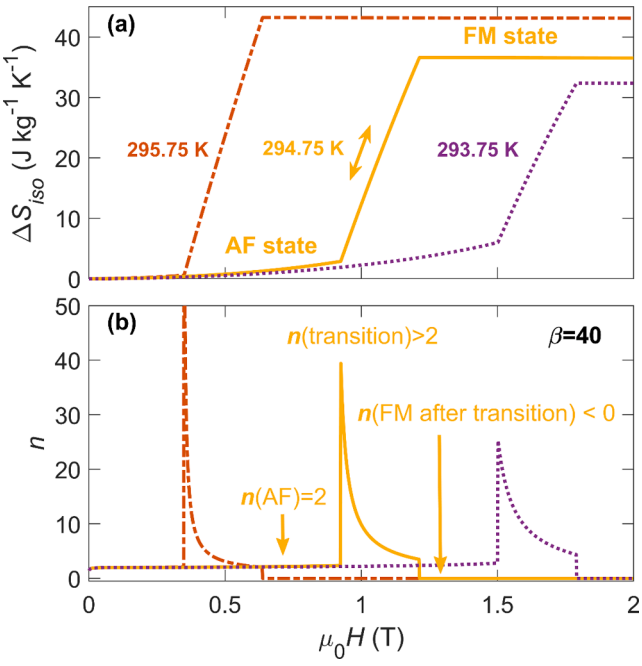

Fig. 5. Field dependence of the isothermal magnetic entropy change (a) and the exponent n (b) for different temperatures close to the transition using $\beta = 40$.

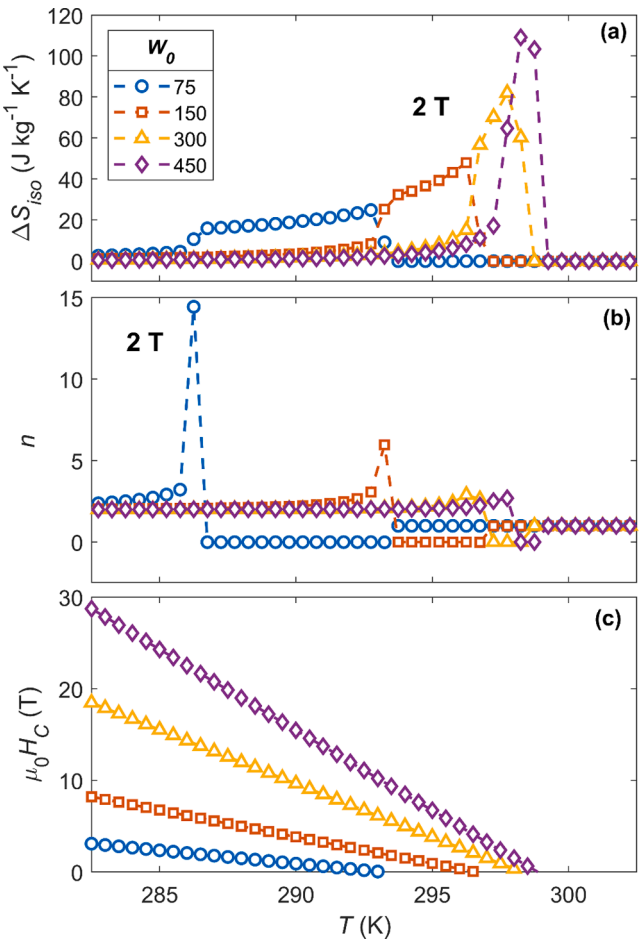

Fig. 6. Temperature dependence of the isothermal magnetic entropy change (a), the exponent n (b) and the critical field (c) for different values of the W_0 parameter using $\beta = 40$.

become smaller as W_0 increases. Moreover, the plateau region after the transition ($n < 0$) become narrower as W_0 is increased. With respect to H_C, it is observed that W_0 is related with the slope and the intercept of H_C vs T, being both variables larger as W_0 increases. It is evident that W_0 strongly modifies $\frac{\partial T_t}{\partial H}$ magnitude, which has a relevant role on the MC properties. From these it can be concluded that, as $\frac{\partial T_t}{\partial H}$ becomes higher, ΔS_{iso} becomes broader but also smaller. Moreover, the square-like shape leads to large overshoot values, as the ΔS_{iso} variation is larger for temperatures below the transition. At this point, it is worth mentioning that though the overshoot values depend on $\frac{\partial T_t}{\partial H}$, the values remain above two in all the cases corresponding to a first order phase transition. The overshoot feature is only dependent on the β parameter.

The effect of the unavoidable FM to PM transition after the AF to FM one on the different properties is analyzed in Fig. 7 for different values of the Curie temperature of the FM state (the AF to FM transition temperature is kept constant at 300 K). It can be observed that the magnetization jump at the AF to FM transition is reduced as the Curie temperature becomes closer; moreover, the AF-FM transition temperature increases with decreasing T_c. This last feature is ascribed to a slower evolution of the critical field as the FM magnetization at the transition decreases (as the high temperature phase is less magnetic, the applied field necessary to stabilize the FM state has to be larger). The reduction in the magnetization change at the AF-FM transition leads to a reduction of ΔS_{iso} values. In the case of the exponent n, the effect of the Curie temperature of the FM phase consists in a reduction of the overshoot values as T_C becomes closer to the AF to FM transition. However, the overshoot is clearly present for all the first order phase transition cases.

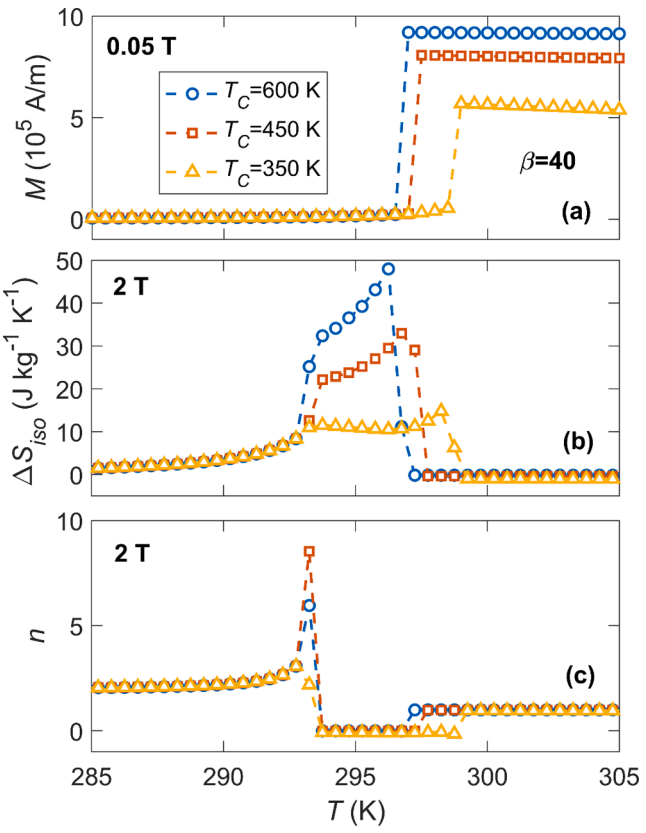

Fig. 7. Temperature dependence of the magnetization (a), isothermal magnetic entropy change (b) and exponent n (c) using $\beta = 40$ for different values of the Curie temperature of the high temperature FM to PM transition.

Experimental results

Although the existence of the overshoot was already observed in experimental data, we will use some of them to illustrate the goodness of the model. First, we discuss the case of a $GdBaCo_2O_6$ sample. The first-order character in this material can be observed from its Arrott plot, for which negative values are observed for temperatures close to the transition. According to Banerjeés criterion, these negative slopes indicate the first-order character of the transition. This material transits from an AF state to a FM one with increasing temperature or magnetic field, without changing the crystal structure (undergoing a magnetoelastic transition, the same as in the model presented here). Fig. 8 shows the temperature and field dependence for ΔS_{iso} (panels **(a)** and **(c)**, respectively) and exponent n (panels **(b)** and **(d)**, respectively) for the $GdBaCo_2O_6$ sample. Both inverse and direct MC responses can be observed, associated to the AF to FM and FM to PM transitions, respectively. Focusing on the inverse effect, ΔS_{iso} increases and shifts to lower temperatures as the magnetic field increases. For the exponent n, the overshoot above 2 can be observed for all the studied fields, increasing as the field increases. This feature, together with the shift of the overshoot to lower temperatures with increasing magnetic field, are in excellent agreement with the model. The values of the overshoot are not so high as for other samples (the next studied sample) indicating a small β or large W_0. Moreover, another feature that is in agreement with the new predictions of the model is the existence of negative values of n close to the transition temperature. The main difference is observed in the value of n in the AF state (around 1.5), which is slightly lower than the expected value of 2. At this point, it should be noted that the magnetization in the model was obtained for perpendicular fields along the easy axis and the effect of parallel fields is not included in this study (and can affect the exponent n in the AF state). Being a polycrystalline

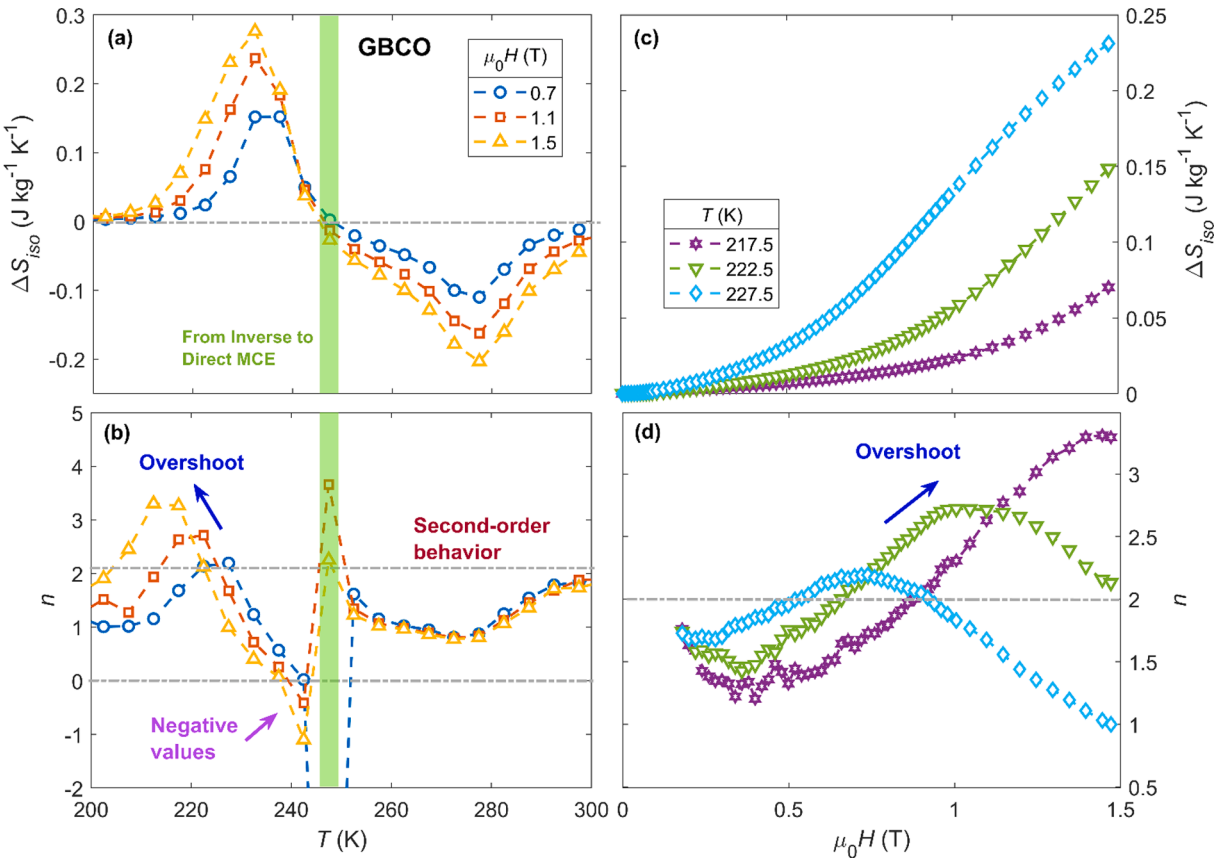

Fig. 8. Temperature dependence of the isothermal magnetic entropy change (a) and the exponent n (b) together with the field dependence of the isothermal magnetic entropy change (c) and the exponent n (d) for the GBCO sample.

sample, the direction of the field with respect to the crystal structure cannot be controlled. Studying the field dependence of both ΔS_{iso} and n magnitudes, similar information can be obtained. For ΔS_{iso} at temperatures below the transition temperature (at 0 field) the values increases as the magnetic field increases, but without reaching saturation (the maximum applied field of 1.5 T is not enough to complete the transformation at that temperatures). For the exponent n, the overshoot is again observed, being shifted to higher magnetic fields as the temperature decreases, in agreement with the model. As the sample does not reach a fully FM state (i.e. the transition is not complete), the negative values after the transition are not observed for those temperatures (see Fig. 8**(d)** and compare to Fig. 5**(b)**). According to this, we can conclude that the main field dependent features of the material can be explained in the frame of the model used. Finally, it should be noted that an extra spike is observed at around 245 K (green highlighted in Fig. 8**(a)** and **(b)**). That feature it is associated to the sign change of ΔS_{iso} (and previously observed in inverse MC materials [27]) and should be neglected from the analysis as it is due to a numerical effect of **Eq.(19).**

We can also compare the results of the model with those of other type of transition, still with an associated inverse MC effect, to see similarities and differences. For that, we selected a $Ni_{49}Mn_{36}In_{15}$ Heusler alloy. This alloy undergoes a martensitic transformation (magnetostructural) from a low magnetization martensitic phase to a high magnetization austenitic one (FM to FM transition). Fig. 9 shows the temperature and field dependence for ΔS_{iso} (panels **(a)** and **(c)**, respectively) and exponent n (panels **(b)** and **(d)**, respectively) for the $Ni_{49}Mn_{36}In_{15}$ sample. For ΔS_{iso} a step-like shape for the temperature dependence can be observed, being quite similar to those modeled in Fig. 4 and indicating low values for W_0 parameter (high values of $\frac{\partial T_t}{\partial H}$). The main difference is the existence of negative values of ΔS_{iso} well below the transition, which are ascribed to the FM character of the martensitic phase. For the exponent n (in which only one field is shown to enhance the visibility of the figure), we can clearly distinguish the overshoot characteristic and the existence of a plateau of negative values at higher temperatures than those of the overshoot associated to the martensitic transition, in agreement to the results of the model. The only difference is the value of n well below the transition which is the corresponding to the FM state (instead of the AF one). With respect to the previous sample, much higher values for the overshoot are obtained. This fact indicates a stronger first-order character in NiMnIn than in GBCO sample (the variation in ΔS_{iso} with the magnetic field is much more pronounced in the former one, Fig. 9**(c)** vs. Fig. 8**(c)**). When analyzing the magnetic field dependence of both ΔS_{iso} and n, again quite similar characteristics to those of the model are observed. This time we can see from ΔS_{iso} that reaching 9 T is enough field to complete the martensitic transformation at the studied temperatures. According to this, it is possible to observe the drop down to negative values of the exponent n at fields above the critical field. This fact, as in the model, is ascribed to the contribution of the FM state after the transition, that has a direct MC response associated to the FM-PM transition that reduces the values of n. Another relevant feature of the martensitic transition at around 220 K (Fig. 9**(b)**), as it was previously observed in the GBCO sample, can be ascribed to a sign change of ΔS_{iso} when the transition starts; this leads to a discontinuity in n from negative to positive values and appears before the overshoot. This discontinuity is more pronounced in the case of NiMnIn sample. Analyzing the field dependence of the exponent n it is evidenced that the discontinuity produces high negative values before the overshoot (Fig. 9**(d)**). This feature is due to the significant contribution of the low temperature (initial) FM phase which produces the change of sign in ΔS_{iso} when the transformation starts (Fig. 9**(c)**). For the GBCO sample there is no sign change from the AF to FM transformation (Fig. 8**(c)**) and then no negative values for n have been observed before the overshoot (Fig. 8

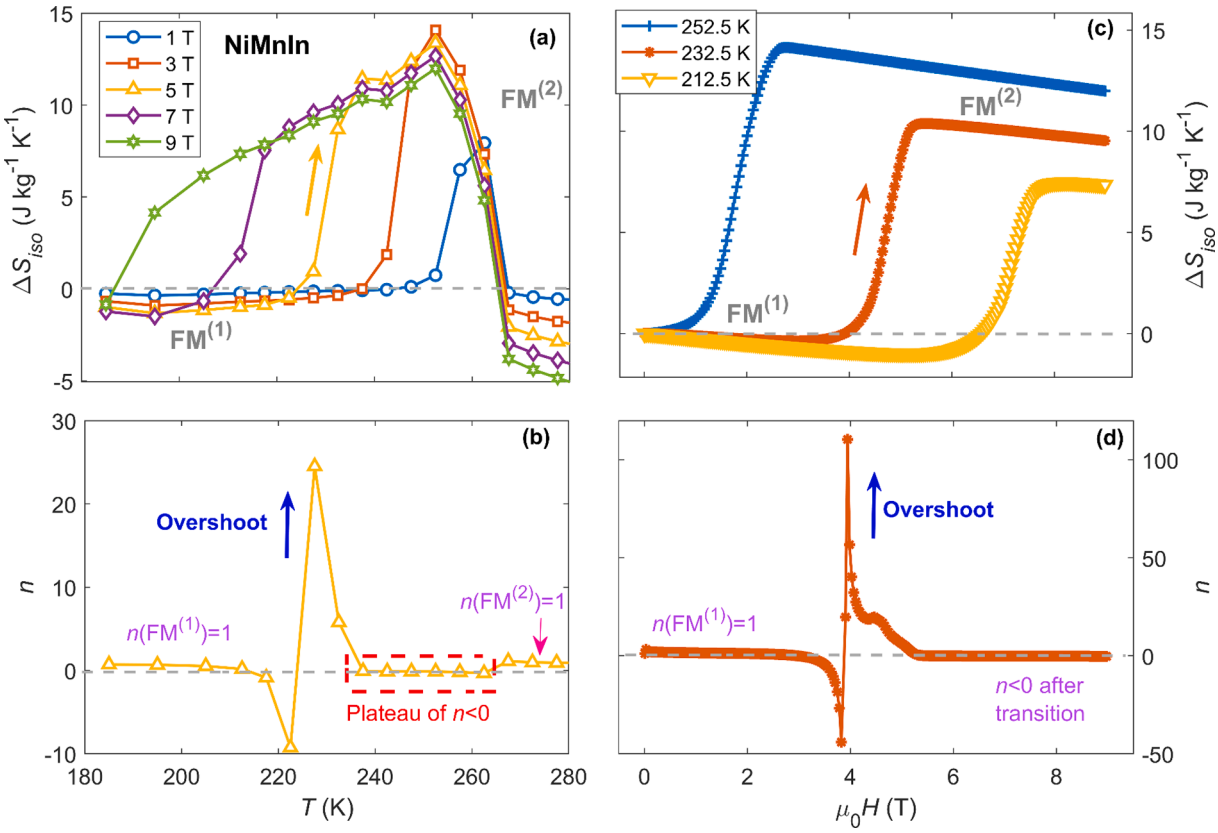

Fig. 9. Temperature dependence of the isothermal magnetic entropy change (a) and the exponent n (b) together with the field dependence of the isothermal magnetic entropy change (c) and the exponent n (d) for the NiMnIn sample.

(d)). It this GBCO sample, the negative values should appear after the overshoot as they are linked to the sign change that this time it is produced by the high temperature (transformed) FM phase (which appears around 245 K, after the overshot, in Fig. 8**(b)**). With this, we reinforce that it is important in experimental data to careful analyze the points where a transition from direct to inverse (or vice versa) response appears, not to misattribute them to an overshoot.

Conclusions

The characteristics of the magnetic field dependence of the isothermal magnetic entropy change ascribed to AF-FM transitions have been theoretically analyzed by means of a mean field approach which incorporates magnetovolume effects. This approach allows us to describe either second- or first-order AF to FM transitions by the modification the magnetovolume coupling parameter (β). In agreement with previous experimental results, the existence of an overshoot above the value of 2 (the one corresponding to a pure AF state) for the exponent n for first-order AF-FM transitions is confirmed theoretically, while no overshoot is observed for second-order ones (no magnetovolume effect, $\beta = 0$). This overshoot is shown to be more prominent as the β parameter increases. For a non-null β parameter, the overshoot is shifted to lower temperatures as the magnetic field increases, and it is shown to be ascribed to the evolution of the transition temperature with the magnetic field and to the abrupt jump in ΔS_{iso} magnitude at low temperatures for first-order materials. Once the AF to FM transition is produced, the direct MC effect associated to the FM phase leads to a slight decrease of the ΔS_{iso} values which produces negative values for the exponent n, never described previously in the literature but present in the experimental data.

These features have been compared to those of experimental data of $GdBaCo_2O_6$, with a good agreement. The analysis can also be extended to $Ni_{49}Mn_{36}In_{15}$ which undergoes a magnetostructural transition with associated inverse MC effect.

Declaration of Competing Interest

The authors declare that they have no known competing financial interests or personal relationships that could have appeared to influence the work reported in this paper.

Acknowledgements

Work supported by AEI/FEDER-UE (grant PID2019-105720RB-I00), US/JUNTA/FEDER-UE (grant US-1260179), Consejería de Economía, Conocimiento, Empresas y Universidad de la Junta de Andalucía (grant P18-RT-746), US Army Research Laboratory under Cooperative Agreement Number W911NF-19-2-0212 and Sevilla University under VI PPIT-US program. L.M.M-R. acknowledges a postdoctoral fellowship from Junta de Andalucía and European Social Fund (ESF). A.K.G. acknowledges support from US Army Research Laboratory's Energy Coupled to Matter–Metals Program.

References

[1] Brown GV. Magnetic heat pumping near room temperature. J Appl Phys 1976;47:3673–80. https://doi.org/10.1063/1.323176.
[2] Zimm C, Jastrab A, Sternberg A, Pecharsky V, Gschneidner K, Osborne M, et al. Description and performance of a near-room temperature magnetic refrigerator. Adv Cryog Eng, Springer, US 1998:1759–66. https://doi.org/10.1007/978-1-4757-9047-4_222.
[3] Kitanovski A, Plaznik U, Tomc U, Poredoš A. Present and future caloric refrigeration and heat-pump technologies. Int J Refrig 2015;57:288–98. https://doi.org/10.1016/j.ijrefrig.2015.06.008.
[4] Tishin AM, Spichkin YI. The magnetocaloric effect and its applications. Elsevier 2016. https://doi.org/10.1887/0750309229.

[5] Langley SK, Chilton NF, Moubaraki B, Hooper T, Brechin EK, Evangelisti M, et al. Molecular coolers: the case for [CuII5GdIII4]. Chem Sci 2011;2:1166. https://doi.org/10.1039/c1sc00038a.

[6] Zhang Y. Review of the structural, magnetic and magnetocaloric properties in ternary rare earth RE2T2X type intermetallic compounds. J Alloys Compd 2019;787:1173–86. DOI:10.1016/j.jallcom.2019.02.175.

[7] Li L, Yan M. Recent progresses in exploring the rare earth based intermetallic compounds for cryogenic magnetic refrigeration. J Alloys Compd 2020;823:153810. DOI:10.1016/j.jallcom.2020.153810.

[8] Wu B, Zhang Y, Guo D, Wang J, Ren Z. Structure, magnetic properties and cryogenic magneto-caloric effect (MCE) in RE2FeAlO6 (RE = Gd, Dy, Ho) oxides. Ceram Int 2021;47:6290–7. https://doi.org/10.1016/j.ceramint.2020.10.207.

[9] Li L, Xu P, Ye S, Li Y, Liu G, Huo D, et al. Magnetic properties and excellent cryogenic magnetocaloric performances in B-site ordered RE2ZnMnO6 (RE = Gd, Dy and Ho) perovskites. Acta Mater 2020;194:354–65. DOI:10.1016/j.actamat.2020.05.036.

[10] Li L, Yuan Ye, Qi Y, Wang Q, Zhou S. Achievement of a table-like magnetocaloric effect in the dual-phase ErZn2/ErZn composite. Mater Res Lett 2018;6:67–71. https://doi.org/10.1080/21663831.2017.1393778.

[11] Franco V, Blázquez JS, Ipus JJ, Law JY, Moreno-Ramírez LM, Conde A. Magnetocaloric effect: from materials research to refrigeration devices. Prog Mater Sci 2018;93:112–232. https://doi.org/10.1016/j.pmatsci.2017.10.005.

[12] Pecharsky VK, Gschneidner Jr KA. Magnetocaloric effect and magnetic refrigeration. J Magn Magn Mater 1999;200:44–56. https://doi.org/10.1016/S0304-8853(99)00397-2.

[13] Pecharsky VK, Gschneidner KA. Giant magnetocaloric effect in Gd5 (Si2 Ge2). Phys Rev Lett 1997;78:4494–7. https://doi.org/10.1103/PhysRevLett.78.4494.

[14] Fujita A, Fujieda S, Hasegawa Y, Fukamichi K. Itinerant-electron metamagnetic transition and large magnetocaloric effects in La(FexSi1-x)13 compounds and their hydrides. Phys Rev B - Condens Matter Mater Phys 2003;67:1044161–10441612. https://doi.org/10.1103/physrevb.67.104416.

[15] Tegus O, Brück E, Buschow KHJ, de Boer FR. Transition-metal-based magnetic refrigerants for room-temperature applications. Nature 2002;415:150–2. https://doi.org/10.1038/415150a.

[16] Planes A, Mañosa Ll, Moya X, Krenke T, Acet M, Wassermann EF. Magnetocaloric effect in Heusler shape-memory alloys. J Magn Magn Mater 2007;310:2767–9. https://doi.org/10.1016/j.jmmm.2006.10.1041.

[17] Franco V, Blázquez JS, Ingale B, Conde A. The magnetocaloric effect and magnetic refrigeration near room temperature: materials and models. Annu Rev Mater Res 2012;42:305–42. https://doi.org/10.1146/annurev-matsci-062910-100356.

[18] Gottschall T, Skokov KP, Fries M, Taubel A, Radulov I, Scheibel F, et al. Making a cool choice: the materials library of magnetic refrigeration. Adv Energy Mater 2019;9:1901322. https://doi.org/10.1002/aenm.201901322.

[19] Franco V, Conde A. Scaling laws for the magnetocaloric effect in second order phase transitions: from physics to applications for the characterization of materials. Int J Refrig 2010;33:465–73. https://doi.org/10.1016/j.ijrefrig.2009.12.019.

[20] Sánchez-Pérez M, Moreno-Ramírez LM, Franco V, Conde A, Marsilius M, Herzer G. Influence of nanocrystallization on the magnetocaloric properties of Ni-based amorphous alloys: determination of critical exponents in multiphase systems. J Alloys Compd 2016;686:717–22. https://doi.org/10.1016/j.jallcom.2016.06.057.

[21] Franco V, Blázquez JS, Conde A. Field dependence of the magnetocaloric effect in materials with a second order phase transition: a master curve for the magnetic entropy change. Appl Phys Lett 2006;89:222512. https://doi.org/10.1063/1.2399361.

[22] Moreno-Ramirez LM, Blazquez JS, Franco V, Conde A, Marsilius M, Budinsky V, et al. A new method for determining the curie temperature from magnetocaloric measurements. IEEE Magn Lett 2016;7:6102004. https://doi.org/10.1109/LMAG.2016.2533481.

[23] Law JY, Franco V, Moreno-Ramírez LM, Conde A, Karpenkov DY, Radulov I, et al. A quantitative criterion for determining the order of magnetic phase transitions using the magnetocaloric effect. Nat Commun 2018;9. https://doi.org/10.1038/s41467-018-05111-w.

[24] Bean CP, Rodbell DS. Magnetic disorder as a first-order phase transformation. Phys Rev 1962;126:104–15. https://doi.org/10.1103/PhysRev.126.104.

[25] Moreno-Ramírez LM, Romero-Muñiz C, Law JY, Franco V, Conde A, Radulov IA, et al. The role of Ni in modifying the order of the phase transition of La(Fe, Ni, Si)13. Acta Mater 2018;160:137–46. https://doi.org/10.1016/j.actamat.2018.08.054.

[26] Moreno-Ramírez LM, Romero-Muñiz C, Law JY, Franco V, Conde A, Radulov IA, et al. Tunable first order transition in La(Fe, Cr, Si)13 compounds: retaining magnetocaloric response despite a magnetic moment reduction. Acta Mater 2019;175:406–14. https://doi.org/10.1016/j.actamat.2019.06.022.

[27] Law JY, Díaz-García Á, Moreno-Ramírez LM, Franco V, Conde A, Giri AK. How concurrent thermomagnetic transitions can affect magnetocaloric effect: the Ni 49 +x Mn 36–x In 15 Heusler alloy case. Acta Mater 2019;166:459–65. https://doi.org/10.1016/j.actamat.2019.01.007.

[28] Law JY, Franco V, Conde A, Skinner SJ, Pramana SS. Modification of the order of the magnetic phase transition in cobaltites without changing their crystal space group. J Alloys Compd 2019;777:1080–6. https://doi.org/10.1016/j.jallcom.2018.11.020.

[29] Li L, Nishimura K, Kadonaga M, Qian Z, Huo D. Giant magnetocaloric effect in antiferromagnetic borocarbide superconductor RNi2B2C (R = Dy, Ho, and Er) compounds. J Appl Phys 2011;110:043912. https://doi.org/10.1063/1.3625250.

[30] Li L-W. Review of magnetic properties and magnetocaloric effect in the intermetallic compounds of rare earth with low boiling point metals. Chinese Phys B 2016;25:037502. https://doi.org/10.1088/1674-1056/25/3/037502.

[31] Annaorazov MP, Nikitin SA, Tyurin AL, Asatryan KA, Dovletov AK. Anomalously high entropy change in FeRh alloy. J Appl Phys 1996;79:1689–95. https://doi.org/10.1063/1.360955.

[32] Chirkova A, Skokov KP, Schultz L, Baranov NV, Gutfleisch O, Woodcock TG. Giant adiabatic temperature change in FeRh alloys evidenced by direct measurements under cyclic conditions. Acta Mater 2016;106:15–21. https://doi.org/10.1016/j.actamat.2015.11.054.

[33] Scheibel F, Gottschall T, Skokov K, Gutfleisch O, Ghorbani-Zavareh M, Skourski Y, et al. Dependence of the inverse magnetocaloric effect on the field-change rate in Mn3GaC and its relationship to the kinetics of the phase transition. J Appl Phys 2015;117:233902. https://doi.org/10.1063/1.4922722.

[34] Krenke T, Duman E, Acet M, Wassermann EF, Moya X, Mañosa L, et al. Inverse magnetocaloric effect in ferromagnetic Ni-Mn-Sn alloys. Nat Mater 2005;4:450–4. https://doi.org/10.1038/nmat1395.

[35] Chernenko VA, L'vov VA, Cesari E, Barandiaran JM. Fundamentals of magnetocaloric effect in magnetic shape memory alloys. In: Brück E, editor. Handb. Magn. Mater., vol. 28, Elsevier; 2019, p. 1–45. DOI:10.1016/bs.hmm.2019.03.001.

[36] L'vov VA, Kosogor A. Inverse magnetocaloric effect in the solids undergoing ferromagnetic – antiferromagnetic phase transition: landau theory applied to Fe-Rh alloys. J Magn Magn Mater 2021;517:167269. https://doi.org/10.1016/j.jmmm.2020.167269.

[37] Callen E, Callen HB. Magnetostriction, forced magnetostriction, and anomalous thermal expansion in ferromagnets. Phys Rev 1965;139:A455–71. https://doi.org/10.1103/PhysRev.139.A455.

[38] Pramana SS, Cavallaro A, Li C, Handoko AD, Chan KW, Walker RJ, et al. Crystal structure and surface characteristics of Sr-doped GdBaCo2O6-: δ double perovskites: oxygen evolution reaction and conductivity. J Mater Chem A 2018;6:5335–45. https://doi.org/10.1039/C7TA06817D.

[39] Zhou L, Mehta A, Giri A, Cho K, Sohn Y. Martensitic transformation and mechanical properties of Ni49+xMn36-xIn15 (x=0, 0.5, 1.0, 1.5 and 2.0) alloys. Mater Sci Eng A 2015;646:57–65. DOI:10.1016/j.msea.2015.08.034.

[40] Landau LD, Pitaevskii LP, Lifshitz EM. Electrodynamics of Continuous Media, Second Edition: Volume 8 (Course of Theoretical Physics) 1984;8:460.

[41] Herpin A. Théorie du magnétisme. Paris: Presses Universitaires de France; 1968.

[42] Kaeswurm B, Franco V, Skokov KP, Gutfleisch O. Assessment of the magnetocaloric effect in La, Pr(Fe, Si) under cycling. J Magn Magn Mater 2016;406:259–65. https://doi.org/10.1016/j.jmmm.2016.01.045.